ChemComm
Chemical Communications

Accepted Manuscript

This article can be cited before page numbers have been issued, to do this please use: Y. Zhuo, L. Wang, M. Jiang, Y. Chai and R. Yuan, *Chem. Commun.*, 2020, DOI: 10.1039/D0CC02207A.

ROYAL SOCIETY OF CHEMISTRY

rsc.li/chemcomm

ROYAL SOCIETY OF CHEMISTRY View Article Online
DOI: 10.1039/D0CC02207A

Journal Name

COMMUNICATION

Intense electrochemiluminescence from organic microcrystals accelerated H_2O_2-free luminol system for microRNA detection

Li Wang, Ming-Hui Jiang, Ya-Qin Chai, Ruo Yuan and Ying Zhuo*

Received 00th January 20xx,
Accepted 00th January 20xx

DOI: 10.1039/x0xx00000x

www.rsc.org/

A kind of organic microcrystals， 9,10-diphenylanthracene microcrystals (DPA MCs) was developed as a novel electrochemiluminescence (ECL) coreactant accelerator to efficiently catalyze dissolved O_2 for more reactive oxygen species (ROSs) generation, achieving intense ECL for H_2O_2-free luminol system. Moreover, based on this ternary ECL system, a signal "off-on" ECL biosensor for microRNA-21 (miRNA-21) detection was constructed combining a sensitive target recycling amplification strategy and the enzyme-mediated recycling strand displacement reaction (RSDR).

Luminol is researched the most commonly and extensively on electrochemiluminescent (ECL) biosensors, owing to its intrinsic advantages of low cost, non-toxic, and highly luminous efficiency.[1] However, its emission is extremely weak in neutral solution and often depends on the help of H_2O_2 as coreactant for signal enhancement. As a result, the dependence on H_2O_2 has suppressed the application of luminol in biological detection, due to the decomposability and instability of H_2O_2.[2,3] Therefore, efficient approaches to develop a H_2O_2-free in luminol-based ECL system is one of the most challengeable work. Dissolved O_2 as an endogenous and innoxious coreactant has drawn great interests. Like H_2O_2, dissolved O_2 can also generate the reactive oxygen species (ROSs), such as superoxide radicals ($O_2^{\bullet-}$), singlet oxygen (O_2^1), and hydroxyl radical ($OH^{\bullet}$),[4] which could react with the radical of the luminol to amplify the ECL signal. Nevertheless, the inherent low reactivity of dissolved O_2 has greatly influenced its use as coreactant to detect the trace substances. Therefore, it is necessary to find a substance that can accelerate the reactivity of dissolved O_2 to produce more ROSs for the ECL signal enhancement in the luminol-dissolved O_2 system.

More recently, we have proposed a new strategy to improve the ECL reaction rate by adding the third substance named coreactant accelerator in the classical binary ECL systems (luminophore/coreactant), which could boost the reactivity of the coreactant to produce more active intermediates for ECL intensity enhancement.[5,6] In the ECL system with dissolved O_2 as coreactant, some noble metal nanomaterials such as porous palladium nanosphere (pPdNSs),[7] and Pt−Ag alloy[8] have been employed as coreactant accelerators due to their excellent electrocatalytic activity towards dissolved O_2. However, the shortage and high cost of noble metals generally hindered their practical application. Thus, it would be a meaningful work to find an economical and accessible material as alternatives to noble metal nanomaterials. 9,10-Diphenylanthracene (DPA) was often used as a common fluorescent and ECL luminophore.[9,10] However, the properties of PAHs that could enrich dissolve O_2 were rarely studied till now.[11,12] Herein, the DPA microcrystals (DPA MCs) were prepared and first acted as coreactant accelerator to achieve intense ECL of luminol.

The quantitative detection of miRNA-21(a biomarker of cancer) is invaluable for early diagnosis of cancer.[13,14] In this work, DPA MCs were first employed as coreactant accelerator in H_2O_2-free luminol system to construct an "off-on" ECL biosensor to detection miRNA-21 with the target recycling amplification strategy and enzyme-mediated recycling strand displacement reaction (RSDR). As described in Scheme 1B, DPA MCs and Au nanoflowers (Au NFs) were assembled on glassy carbon electrode (GCE) successively for the immobilization of the S3 strand through the Au-S bond. Then, the dopamine (DA) labelled S4 strand (S4-DA) was hybridized with S3, which presented the "signal off" state to obtain the low background signal, due to the quenching effect of DA. To achieve the target recycling amplification, the "Y"-DNA structures (Y-DNA) were labelled on the Au@Fe_3O_4 through the Au-S bond and reacted with miRNA-21 to release the mimic targets S0 (MT). Meanwhile, with the participation of adenosine triphosphate (ATP), the recycling of miRNA-21 would trigger by the specific binding of ATP and S2 (scheme 1A). Finally, the MT was released and introduced to the sensing surface and initiated the RSDR with the assistance of T7 Exonuclease (T7 Exo) to achieve the "signal on" state. The constructed biosensor not only exhibited high sensitivity for miRNA detection but also presented a new kind of signal amplification strategy in H_2O_2-free luminol system.

Chongqing Engineering Laboratory of Nanomaterials & Sensor Technologies, College of Chemistry and Chemical Engineering, Southwest University, Chongqing 400715, China.

E-mail: yingzhuo@swu.edu.cn.(Y. Zhuo).
Fax: +86-23-68253172; Tel: +86-23-68253172
Electronic Supplementary Information (ESI) available: Experimental Section; ECL Characterization of the Proposed Biosensor; Electrochemical Characterization of the Proposed Biosensor； Optimization of the reaction condition.
See DOI: 10.1039/x0xx00000x

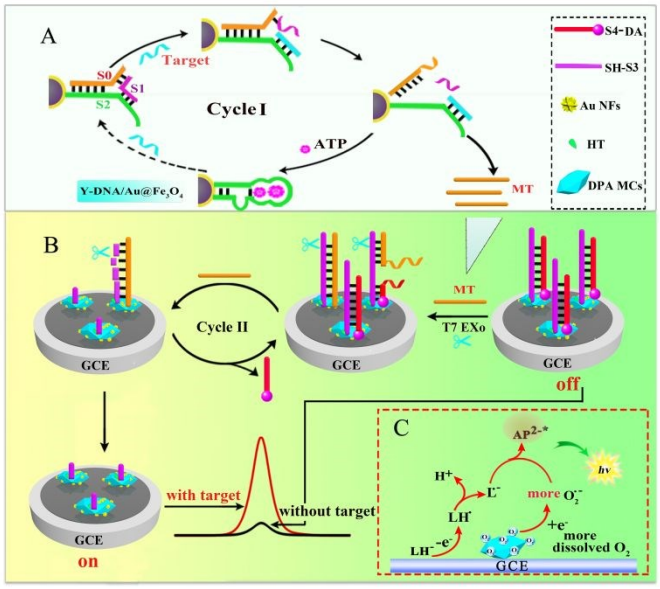

Scheme 1. Schematic representation of (A) the target recycling amplification process, (B) the reaction process of the proposed biosensor and (C) the possible mechanism of the luminol/dissolved O_2/DPA MCs ternary ECL system.

The target-recycling amplification process (cycle I, Scheme1) and the enzyme-assisted cycling strand displacement reaction (RSDR, cycle II, Scheme1) were successfully confirmed through a PAGE experiment. As showed in lane 3 (Fig. 1A, a), when the target cycle amplification strategy occurred with the help of ATP, it was surprisingly found that the supernatant contained the band of MT. However, there was no band in lane 4 when there was only with ATP but without target, indicating that the target cycle amplification strategy could induce only when the target existed for generating the MT. The lane 2 showed the cleavage product S4 (Fig. 1A, b), when the S3-S4 duplex, S0 and 100 U/mL T7 Exo were mixed together. These results had confirmed the feasibility of our method.

In order to compare the ECL performance of our system with that of the traditional luminol/H_2O_2 binary ECL system, a comparative experiment was carried out. As displayed in Fig. 1B, the ECL intensity of luminol/H_2O_2 binary ECL system was approximately 8456 a.u. (blue line). However, the ECL intensity of luminol/dissolved O_2/DPA MCs ternary ECL system was reached at 13303 a.u. (red line), which was 15.8% higher than that of the luminol/H_2O_2 binary system, which open new opportunities for design of more H_2O_2-free luminol ECL system.

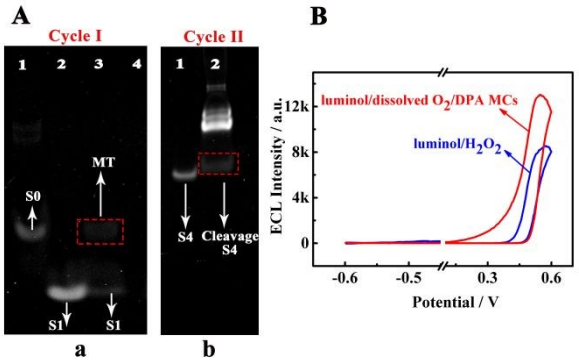

Fig. 1 (A) PAGE analysis of the samples: Cycle I (lane 1, 2 μM S0; lane 2, 2 μM S1, lane 3, the supernatant containing (2 μM) and ATP (10 μM) ; lane 4, the supernatant containing ATP and in the absence of miRNA-21); cycle II (lane 1, 2 - μM S4; and lane 2, the mixture of S3-S4 (2 μM), S0 (2 μM), 100 U/mL T7 Exo with incubating at 37 °C for 2 h before PAGE). (B) ECL response of luminol/dissolved O_2/DPA MCs ternary ECL system (red line) and luminol/H_2O_2 binary ECL system (blue line). The corresponding concentration of luminol solution and H_2O_2 solution was 30 μM and 2 mM, respectively.

The scanning electron microscopy (SEM) technology was utilized to characterize the morphologies and sizes of different materials. The DPA MCs possessed special structure of capsule with 2 ± 1 μm long and 500 ± 200 nm wide (Fig. 2A). Fig. 2B was the high-magnification SEM image of DPA MCs, in which the uniform octagon shapes of DPA MCs were exhibited, which provided a good evidence that DPA MCs was a kind of microcrystal. Fig. 2C displayed the SEM image of Au NFs formed ~200-nm-diameter ball structures, and their surfaces exhibited many distinct wrinkles, demonstrating the abundant active sites on Au NFs surface for subsequent electrode modification. Finally, the Fig. 2D displayed the SEM image of Au@Fe_3O_4, which showed the 16 nm Au NPs were distributed on the surface of the spherical structures of Fe_3O_4 nanoparticles.

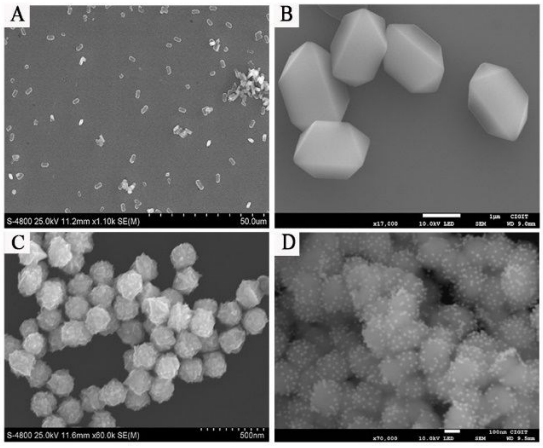

Fig. 2 SEM images of (A) DPA MCs, (B) local magnification of DPA MCs, (C)Au NFs, and (D) Au@Fe_3O_4.

ECL-potential curves, cyclic voltammetry (CV) and 3D ECL spectra were conducted to investigate the possible mechanism of the proposed ECL system. As showed in Fig. 3A, the DPA MCs/GCE didn´t presented any ECL response in the PBS solution (curve *a*), indicating that DPA MCs could not be acted as luminophore under this potential window. When the bare GCE was measured in air-saturated luminol solution, the ECL intensity increased to 2400 a.u. (Fig. 3A, curve *b*). It manifested that the ECL signal was originated from luminol with dissolved O_2 as an endogenous coreactant,[15] which could generate ROSs (such as $O_2^{\bullet-}$, $OH^{\bullet}$ and O_2[1] et al) to react with the active intermediates of oxidized luminol. Surprisingly, the ECL signal of DPA MCs/GCE in air-saturated luminol solution was significantly increased to 13033 a.u. (Fig. 3A, curve *c*), revealing that the DPA MCs could effectively enhance the ECL signal of luminol with the coreactant of dissolved O_2. As illustrated in Fig. 3C, the characteristic ECL emission wavelength of luminol solution was located at 417 nm, which was corresponding to the previous literature.[16] When DPA MCs/GCE was measured in luminol solution, the ECL signal significantly ascended and the characteristic ECL wavelength was also at 417nm, which revealed that the luminophore was still luminol (Fig. 3D). Thus, it was concluded that DPA MCs could enhance the ECL signal of H_2O_2-free luminol system and play the role of coreaction accelerator due to the enrichment of dissolved O_2 on its surface,

where they may accelerate the reduction reaction of dissolved O_2 to generate more $O_2^{\bullet-}$.[11,12] It was worth mentioning that the novel luminol/dissolved O_2/DPA MCs ternary ECL system had higher ECL intensity than that of the traditional luminol/H_2O_2 binary system, which sheds light on the development of sensitive H_2O_2-free luminol system. To further explore the interaction between DPA MCs and dissolved O_2, ECL-potential curves and CV curves were investigated. When the DPA MCs/GCE was tested in N_2-saturated luminol solution (Fig. 3A, curve *d*), the ECL emission decreased compared with that of air-saturated luminol solution (Fig. 3A, curve *c*), revealing the crucial role of dissolved O_2 as the coreactant of luminol for ECL amplification. After adding the dimethyl sulfoxide (DMSO) to scavenge the $OH^{\bullet}$ in the luminol solution[17] (Fig. 3A, curve *e*), the ECL response had no change compared with curve *c* in Fig. 3A. Successively, when p-benzoquinone as a good scavenger for $O_2^{\bullet-}$ was added into the luminol solution[18] (Fig. 3A, curve *f*), the ECL intensity decreased dramatically from 13303 to 1770 a.u.. These results indicated that the $O_2^{\bullet-}$ produced by dissolved O_2 has participated directly in the ECL emission rather than $OH^{\bullet}$. Meantime, the corresponding CVs were performed to further explore the reaction mechanism between DPA MCs and dissolved O_2. According to Fig. 3B, the redox peaks can be seen from the CV curve of DPA MCs/GCE in the air-saturated KOH solution (0.1M, curve *a*), which were not exhibited in N_2-saturated KOH solution (curve *b*). Besides, neither the CV curves of bare GCE nor DPA MCs/GCE in N_2-saturated 0.1M KOH solution had no redox peaks (Fig. 3B, curve *c* and *d*) due to the lack of dissolved O_2. The above results verified that the DPA MCs could catalyze the redox reaction of dissolved O_2.

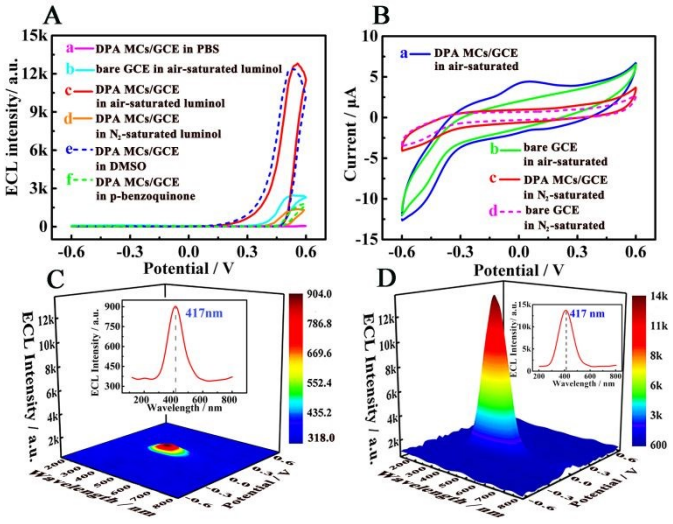

Fig. 3 (A) ECL-potential curves of (a) DPA MCs/GCE in PBS, (b) bare-GCE and (c) DPA MCs/GCE in air-saturated luminol solution, (d) DPA MCs/GCE in N_2-saturated luminol solution, (e) DPA MCs/GCE in air-saturated luminol solution containing 10 mM DMSO and (f) in air-saturated luminol solution containing 1 mM p-benzoquinone. (B) The CV curves of (a) DPA MCs/GCE, (b) bare-GCE in air-saturated KOH solution and (c) DPA MCs/GCE, (d) bare-GCE in N_2-saturated KOH solution. C) and (D) were the 3D ECL spectra spectrum of bare GCE and DPA MCs/GCE in air-saturated luminol solution. The concentration of luminol solution and KOH solution was 30 μM, 0.1 M, respectively.

As a result, the DPA MCs as coreaction accelerator in luminol/dissolved O_2 system could enhance the ECL with good catalytic performance of dissolved O_2 to produce more $O_2^{\bullet-}$. The $O_2^{\bullet-}$ and luminol anion radical ($L^{\bullet-}$) interacted to promote the ECL.[19] Firstly, $L^{\bullet-}$ was generated by luminol anion (LH^-) electrochemical oxidation, then DPA MCs aggregated more dissolved O_2 on its surface and catalytically reduce them to $O_2^{\bullet-}$. Finally, $L^{\bullet-}$ and $O_2^{\bullet-}$ would react to generate a large amount of excited state species 3-aminophthalate (AP^{2-*}) to obtain an excellent ECL emission. The corresponding mechanism were listed in Scheme 1 (C).

The performance of fabricated biosensors was assessed by recording the ECL responses to miRNA-21 with a series of different concentrations. As displayed in Fig. 4A, the ECL signals enhanced with the increase of miRNA-21 concentration (from 100 aM to 100 pM). In addition, from Fig. 4B, a good linear relationship was exhibited between the concentration of miRNA-21 and the ECL signals. The regression equation was fitted as $I = 24038.53 + 1314.9 \lg c$ (correlation coefficient $R = 0.9965$) and the detection limit was calculated as 18.3 aM (S/N = 3). Moreover, as can be seen from Table S2, the proposed biosensor had a wider detection range and a lower detection limit than that of other methods for the miRNA-21 detection.

We further investigated the performance of the proposed biosensor. First, 6 different kinds of miRNAs including miRNA-141 (100 pM), miRNA-let-7a (100 pM), miRNA-155 (100 pM), miRNA-182-5p (100 pM), miRNA-126 (100 pM), and miRNA-199a (100 pM) were selected as interfering substances to execute comparative experiments. As described in Fig. 4C, the ECL signals with interfering miRNAs presented no differences compared with the result of the blank test (using PBS instead of miRNA-21 solution to execute the target recycling amplification strategy). Moreover, the mixed solution (100 pM of the above six kinds of miRNAs containing 1pM of miRNA-21) showed a remarkable ECL enhancement, demonstrating that the proposed ECL biosensor possessed an excellent selectivity. Furthermore, the stability of proposed biosensor was assessed *via* successive scans for 23 cycles at 10 fM of miRNA-21. As seen from Fig. 4D, the ECL signals kept steady enough with relative standard deviations (RSD = 1.08%). The results suggested that the proposed biosensor had an admirable stability.

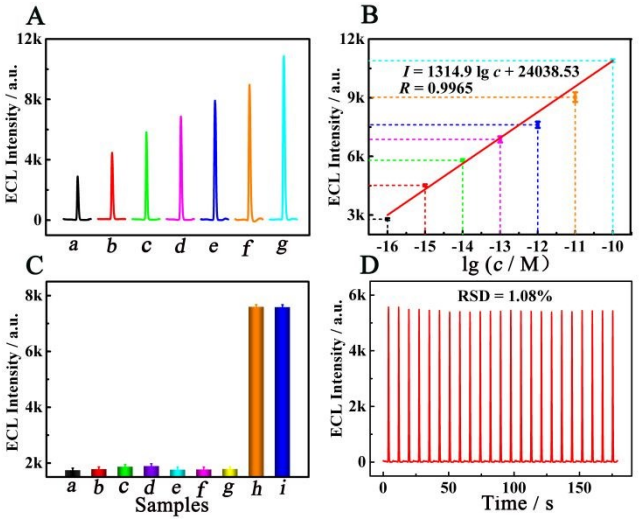

Fig. 4 (A) ECL response of the proposed biosensor to different concentrations of miRNA-21: 100 aM, 1 fM, 10 fM, 100 fM, 1 pM, 10 pM, 100 pM (from a to g). (B) The calibration plot of ECL response versus the logarithm of miRNA-21. (C) Selectivity of the developed biosensor toward various miRNA (*a*:blank; *b*:miRNA-141; *c*:miRNA-155; *d*:miRNA-199a; *e*:miRNA-126; *f*:miRNA-182-5p; *g*:miRNA-let-7a; *h*:miRNA-21; *i*:mixture) and (D) Stability of the constructed biosensor through successive scans with 23 cycles (miRNA-21 concentration at 10 fM).

In order to investigate the feasibility of the proposed method. The lysates of human cervical cancer cells (HeLa) and human breast cancer cells (MCF-7) were selected for ECL assay to measure miRNA-21 expression. The ECL signals was studied by setting the cell concentration from 10 cells to 1×10^5 cells. As can be seen from Fig.5 the ECL signals gradually improved with the

cell numbers of MCF-7 increased from 10 cells to 10^5 cells, validating the miRNA-21 exhibited high expression in MCF-7 cells. However, there was no ECL signal changes in HeLa cells, which completely showed that miRNA-21 was low expression in HeLa cells. The results are consistent with the previous work,[20] indicating that the biosensors constructed in this system could detect miRNA-21 in cancer cells. As the full development of efficient circulating tumor cells enrichment and single tumor cell analysis in the peripheral blood,[21] we believe that the constructed biosensor in our work would have a meaningful impact on the analysis of peripheral blood specimens.

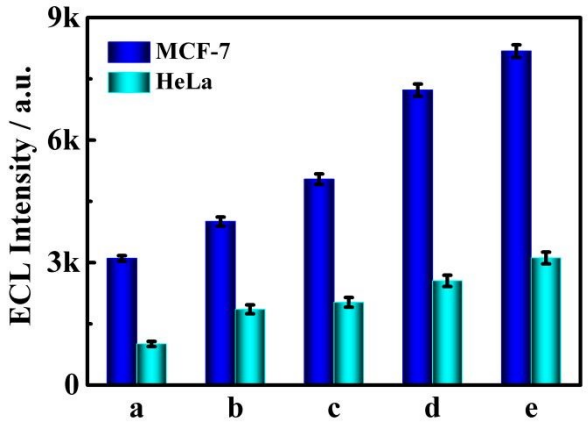

Fig. 5 The real sample analysis of miRNA-21 was performed with different concentrations of different cell lysates: (a) 10 cells, (b) 1×10^2 cells, (c) 1×10^3 cells, (d) 1×10^4 cells and (e) 1×10^5cells of human cervical cancer cells (HeLa) and human breast cancer cells (MCF-7), respectively.

In summary, the DPA MCs acted as a new coreaction accelerator, had achieved intense ECL in the H_2O_2-free luminol system, which would provide a desirable biosensing platform with high selectivity and sensitivity for miRNA-21 detection with the low detection limit of 18.3 aM. It could be attributed to the enrichment of dissolved O_2 on DPA MCs surface to accelerate the reduction reaction of dissolved O_2 for more $O_2^{\bullet-}$ generation, which could react with luminol anion radical ($L^{\bullet-}$) for ECL enhancement. We believe this success would not only provide new insights to expand the applications of DPA MCs but also yield more clues into the present H_2O_2-free luminol ECL system.

Acknowledgement

This work was financially supported by the NNSF of China (21675130, and 21775124), the Natural Science Foundation Project of CQ CSTC (cstc2018jcyjAX0546) and Fundamental Research Funds for the Central Universities (XDJK2019TJ002), China.

Conflicts of interest

There are no conflicts to declare.

Notes and references

1. C. Ma, Y. Cao, X. D. Gou, and J. J. Zhu, *Anal. Chem.*, 2020, **92,** 431-454.
2. T. T. Zhang, Y. Gu, C. Li, X. Y. Yan, N. N. Lu, H. Liu, Z. Q. Zhang, and H. Zhang, *ACS Appl. Mater. Interfaces* 2017, **9**, 37991−37999.
3. Z. M. Hu, X. Jiang, F. J. Xu, J. Jia, Z. Long, X. D. Hou, *Talanta.*, 2016, **158**, 276–282.
4. E. W Miller, O. Tulyathan, E. Y Isacoff, C. J. Chang, *Nat. Chem. Biol.*, 2007, **3**, 263–267.
5. Y. M. Lei, R. X. Wen, J. Zhou, Y. Q. Chai, R. Yuan, and Y. Zhuo, *Anal. Chem.*, 2018, **90**, 6851−6858.
6. F. Yang, X. Y. Jiang, W. B. Liang, Y. Q. Chai, R. Yuan, and Y. Zhuo, *Anal. Chem.*, 2020, **92**, 2566−2572.
7. S. S. Yang, M. H. Jiang, Y. Q. Chai, R. Yuan, and Y. Zhuo, *ACS Appl. Mater. Interfaces* 2018, **10**, 38648−38655.
8. J. L. Liu, Z. L. Tang, J. Q. Zhang, Y. Q. Chai, Y. Zhuo, and R. Yuan, *Anal. Chem.*, 2018, **90**, 5298−5305.
9. K. M. Omer, S. Y. Ku, J. Z. Cheng, S. H. Chou, K. T. Wong, and A. J. Bard, *J. Am. Chem. Soc.*, 2011, **133** ,5492–5499.
10. K. M. Omer, S. Y. Ku, K. T. Wong, and A. J. Bard, *Angew. Chem., Int. Ed.*, 2009, **48**, 9300 –9303.
11. S. N. Chu, S. Sands, M. R. Tomasik, P. S. Lee, and V. F. McNeill, *J. Am. Chem. Soc.*, 2010, **132**, 15968-15975.
12. F. Giroud, S. D. Minteer, *Electrochem. Commun.*, 2013, **34**, 157–160.
13. P. Z. Qin, L. Yao, J. G. Xu, G. D. Liu and W. Chen, *Chem. Commun.*, 2019, **55**, 14367-14370.
14. X. J. Yang, M. R. Cui, X. L. Li, H. Y. Chen and J. J. Xu, *Chem. Commun.*, 2020, **56**, 2135-2138.
15. X. L. Cai, B. Zheng, Y. Zhou, M. R. Younis, F. B. Wang, W. M. Zhang, Y. G. Zhou, X. H. Xia, *Chem. Sci.*, 2018, **9**, 6080-6084. 18
16. J. W. Gao, M. M. Chen, W. Wen, X. H. Zhang, S. F. Wang and W. H. Huang, *Nanoscale*, 2019, **00**, 1-9.
17. T. T. Chen, Y. H. Hu, Y. Cen, X. Chu, and Y. Lu, *J. Am. Chem. Soc.*, 2013, **135,** 11595-11602.
18. Z. L. Han, J. N. Shu, Q. S. Jiang, and H. Cui, *Anal. Chem.* 2018, **90**, 6064−6070.
19. W. L. Gu, H. J. Wang, L. Jiao, Y. Wu, Y. X. Chen, L. Y. Hu, J. M. Gong, D. Du and C. Z. Zhu, *Angew. Chem., Int. Ed.*,2020, **59**, 3534-3538.
20. Z. M. Ying, Z. Wu, B. Tu, W. H. Tan, J. H. Jiang, *J. Am.Chem. Soc.*, 2017, **139,** 9779−9782.
21. C. L. Chaffer, and R. A. Weinberg, *Science*, 2011, **331**, 1559.

embeFor only TOC